Enhanced Photo-Induced Property of LPCVD-TiO$_2$ Layer on PCVD-TiO$_x$ Initial Layer

Satoshi Yamauchi, Keisuke Yamamoto, Sakura Hatakeyama*

Department of Biomolecular Functional Engineering, Hitachi, Japan
Email: ysatoshi@mx.ibaraki.ac.jp

Abstract

Plasma-assisted chemical vapor deposition (PCVD) was applied for amorphous TiO$_x$ deposition on Pyrex-glass substrate at low temperature below 90°C to control orientation of anatase-TiO$_2$ layer by low pressure chemical vapor deposition (LPCVD) using TTIP-single precursor. Preferentially <112>-oriented anatase-TiO$_2$ layer was successfully deposited with the orientation ratio as high as 68% on the initial layer of the thickness around 70 nm. Contact angle water was quickly decreased by UV-irradiation on the highly <112>-oriented TiO$_2$ layer comparing with the layer directly deposited on glass, whereas surface roughness on the former was significantly reduced in comparison to that on the latter. Methyleneblue (MB) aqueous solution with the concentration of 2 mmol/L was used to evaluate photocatalytic property on the layer. Rate constant of MB-decomposition via first order kinetics increased with the orientation ratio above 60% was resulted in 2.3 × 10^{-1} min^{-1} for the layer with <112>-orientation ratio of 68%, whereas the constant was 2.8 × 10^{-3} min^{-1} for the layer directly deposited on glass.

Keywords

LPCVD Anatase-TiO$_2$, PCVD TiO$_x$, Hydrophilicity, Photocatalyst

1. Introduction

Anatase-TiO$_2$ with wide energy bandgap about 3.2 eV has been well recognized as useful material for photo-induced application using the hydrophilic property and the catalytic reactions [1] [2]. Since the property is dependent on the crystallinity including the surface defects, the surface roughness, the orientation, the dopant and

---
*Sakura Hatakeyama now belongs with Hitachi Industry & Control Solutions, Ltd.

so on, a lot of process has been extensively studied for synthesis of anatase-TiO_2. In general, the powder consisting of nano-particles has been used to decompose organic compounds in aqueous solution by UV-irradiation, in which the particle size, the dopant, the defects etc. have been studied to enhance the decomposition efficiency [3]-[5]. On the other hand, sol-gel, reactive sputtering, vacuum evaporation, chemical vapor deposition and so on have been also studied to fabricate anatase-TiO_2 layer [6]-[8], in which the orientation, the surface roughness, the defects etc. are expected to be control in addition to fabrication of the multilayer [9]. Especially, chemical vapor deposition (CVD) with great merit for conformal formation of the layer on three-dimensionally structured surface is so useful to control the orientation. Previously, Tokita *et al.* demonstrated <112>, <110>, <100> and <001>-oriented epitaxial growth of anatase-TiO_2 layer deposition by CVD using titanium-tetra-iso-propoxide (TTIP) on C-sapphire, (110)MgO, (100)MgO and (100)$SrTiO_3$ single crystal, respectively, and efficient decomposition of methyleneblue on (112)anatase-TiO_2 by UV-irradiation in comparison to other oriented layers [10]. Kim *et al.* showed that <112>-orientation ratio in poly-crystalline anatase-TiO_2 layer could be increased at 360˚C on Soda-lime glass by CVD, in which benzene decomposition rate under UV-irradiation on the layer preferentially oriented toward <112> was higher than that on <001>-preferred layer depending on the layer thickness [11]. Here, the demonstrated process to form <112>-oriented anatase-TiO_2 layer on Soda-lime glass has an advantage for the industrial product but impurities are diffused into the layer from the substrate. On the other hand, poly-crystalline anatase-TiO_2 layer consisting of <110>, <100> and <211>-oriented grains can be formed on Pyrex-glass and quartz by CVD [12] [13]. However, the control of orientation has not been achieved yet whereas the previous report suggested <112>-oriented anatase-TiO_2 is useful for efficient photocatalyst.

In this paper, initial TiO_x layer deposited by plasma-assisted CVD (PCVD) at low temperature below 90˚C is used to control of the orientation of anatase-TiO_2 layer on Pylex-glass by low-pressure CVD (LPCVD) using TTIP-single precursor, and then the UV-induced hydrophilic property and the photocatalytic property in methyleneblue solution are demonstrated by using the LPCVD-TiO_2 layer.

2. Experimental

2.1. Deposition of TiO_x and TiO_2 Layers

Figure 1(a) shows an apparatus for deposition of TiO_x and TiO_2 layers. Base pressure of the bell-jar type reactor exhausted by a combination of diffusion pump and a rotary pump was under 1×10^{-3} Pa. TTIP (Ti(O-i-C_3H_7)$_4$: 99.7%-purity) purified in vacuum was used as source gas. Details of the purification sequence of TTIP were already shown elsewhere [12]. TTIP vaporized at 65˚C was introduced into the reactor by using a variable valve with monitoring the reactor pressure by Schulz gage and supplied to substrate through a quartz tube of 12 cm$^\Phi$. An orifice consisting of stainless sheet with a hole of 1 mm$^\Phi$ as shown in **Figure 1(b)** was attached at the gas inlet of Schulz gage and heated at 450˚C by resistive heating to avoid TiO_x deposition on the electrodes due to
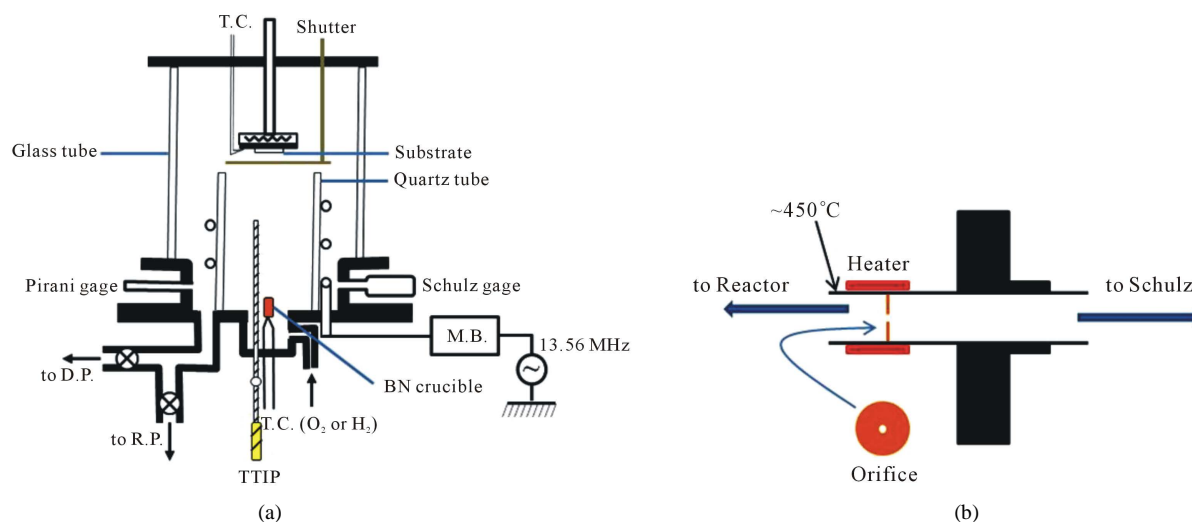

Figure 1. Configuration of (a) apparatus of TiO_x and TiO_2 layers and (b) orifice to avoid TiO_x-deposition on electrode of Schulz gage.

the dissociation of TTIP. In the case of PCVD, 13.56 MHz radio-frequency power of 50 W was applied through inductively coupled electrode around the quartz tube. The reactor pressure during PCVD and LPCVD was controlled at 2.5×10^{-1} Pa and 2.2×10^{-1} Pa, respectively. In the both case, any guest gas such as O_2 and H_2 was not used for the depositions. Optically flat Pyrex-glass with 1 mm-thick was used as substrate, which was mounted on a substrate holder after chemical cleaning by organic solvents and thermally cleaned at 250˚C for 1 hr in vacuum. Temperature of the substrate holder and TTIP gas-inlet line were increased by controlled by PID-systems using thermo-couples and resistive heating.

2.2. Evaluation

Thickness and surface roughness (Ra) of PCVD-TiO$_x$ and LPCVD-TiO$_2$ layers were checked by a surface profiler (Veeco, DEKTAK150). Crystallographic property was examined by θ - 2θ X-ray diffraction (XRD) using Cu-K$_{\alpha 1}$ and K$_{\alpha 2}$ (Rigaku RAD-B). Optical emission spectroscopy of plasma in reactor was carried out by UV-Vis spectrometer (OCEAN OPTICS: USB-2000) though a quartz-window. Hydrophilicity on the TiO$_2$ layer was evaluated by contact angle of deionized water (10 μL) dropped on the layer at 20˚C in 50%-humidity, in which UV-light with the power density of 0.5 mW/cm^2 was irradiated on the layer using a 365 nm black-light. Methyleneblue (MB) aqueous solution with the concentration of 2 mM (mmol/L) in deiozied water was prepared to evaluate photo-induced catalytic property on TiO$_2$ layer, in which the solution was filled in cell consisting of 1 mm-thick quartz-plate and 200 μm-thick spacer with a 1 cm × 1 cm window and then capped by LPCVD-TiO$_2$ layer deposited on Pyrex-glass. Configuration of the setup to monitor the absorption intensity due to MB during UV-light irradiation is shown in **Figure 2**. UV-light around 365 nm selected from Hg-Xe UV-light by a bandpass filter was irradiated on TiO$_2$ layer with the power density of 2 mW/cm^2 through a quartz plate and the quartz cell. He-Ne laser light with the wavelength of 623 nm was simultaneously introduced into the UV-light pass-line by using the quartz plate, and the light through the sample and a UV-cut filter was detected by a Si-photodiode biased at 4 V in the reverse side, then the signal from the photodiode was recorded by PC using A/D converter. Optical power of the laser-light in front of the cell was 180 μW. Transmittance of the laser-light was calibrated by the intensity when deionized water was filled in the sample cell.

3. Results and Discussions

3.1. Anatase-TiO$_2$ Deposition by LPCVD Using TTIP Single Precursor

Figure 3 in Arrhenius plot shows temperature dependent deposition rate by LPCVD using TTIP-single precursor.
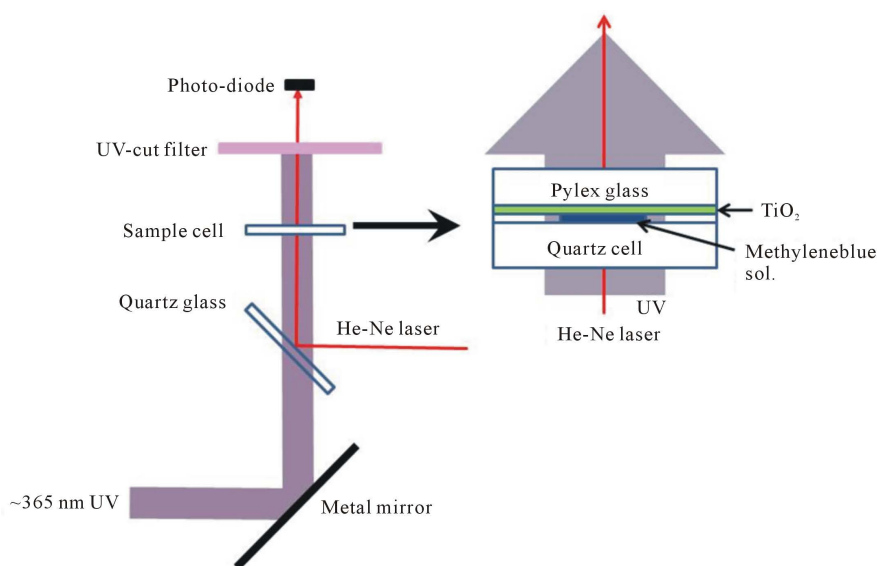

Figure 2. Optical setup to evaluate MB-decomposition, in which the power of UV-light around 365 nm and He-Ne laser at 633 nm was 2 mW/cm^2 and 160 μW on TiO$_2$ layer respectively.
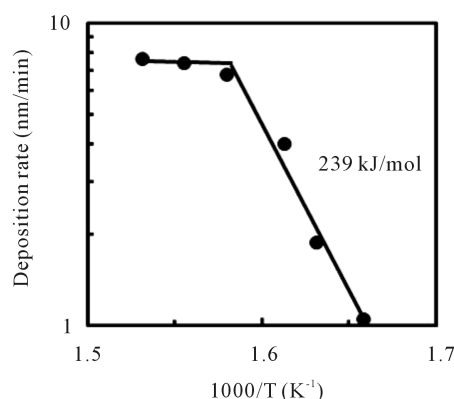
Figure 3. Deposition rate of LPCVD-TiO$_2$ layer for the deposition temperature in Arrhenius plot.

The deposition rate was increased with temperature and saturated above 360˚C, which was similar to the deposition by using TTIP + O$_2$ [12] and TTIP + H$_2$ [13]. Activation energy obtained as 239 kJ/mol for the deposition in surface reaction region (≤360˚C) was in agreement with the energy for the deposition by TTIP + H$_2$ (238 kJ/mol) [14]. Since the deposition rate is promised to be limited by TTIP-dissociation, the activation energy is owing to the barrier for TTIP-dissociation. Previously, Shimakov *et al.* simulated TTIP-dissociation scheme by quantum chemical calculations using Gaussian 03 at B3LYP/6-311++G(2df, p) level, and suggested effective activation barrier for monomolecular TTIP-dissociation to form Ti(OC$_3$H$_7$)$_3$(OH) and propene is 56.9 kcal/mol (238 kJ/mol) [14]. The calculated energy was in good agreement with the experimentally obtained value of 239 kJ/mol, which indicated the LPCVD using TTIP single precursor in surface reaction region was limited by the TTIP-dissociation scheme. As Ti(OC$_3$H$_7$)$_3$(OH) is formed on the substrate, the following oxolation reaction similar to sol-gel process using TTIP is easily expected on the surface;

$$(RO)_3Ti\text{-}OH + XO\text{-}Ti(OR)_3 \rightarrow (RO)_3Ti\text{-}O\text{-}Ti(OR)_3 + XOH\uparrow, (R = C_3H_7, X = R \text{ or } H).$$

In this work, LPCVD-TiO$_2$ layers to examine the crystallographic and photo-induced properties were deposited at 360˚C.

3.2. TiO$_x$ Deposition by PCVD Using TTIP Single Precursor

Figure 4 shows optical emission spectrum of RF-plasma when TTIP was introduced into the reactor. Typical emissions due to H- and H$_2$-radicals were observed with CO-radicals but the emission originated from O, O$_2$ and OH was not detected in the plasma. In the case that oxidant species such as oxygen or hydroxyl enhance TTIP-dissociation in TiO-R bond, CO and CO$_2$ is formed in the plasma [15]. However, the spectrum without the peak due to the oxidants indicated TTIP was partially dissociated in Ti-OR bond and CO formed by cracking of the dissociated OR, which was resulted in Ti-rich (O-poor) TiO$_x$ layer deposition linearly increasing the thickness with the deposition period as shown in **Figure 5**. It is noted that the PCVD was performed at low temperature below 90˚C, therefore, the as-deposited TiO$_x$ layer was formed in amorphous-phase but the surface was partially crystallized just before TiO$_2$ deposition by LPCVD because ring-pattern in halo was slightly observed by RHEED observation for the TiO$_x$ layer annealed at 360˚C in vacuum depending on the TiO$_x$ thickness whereas the ring was not observed for the as-deposited layer. Details of the crystallization feature are in progress by TEM analysis. In this work, LPCVD was successively performed in reactor on PCVD-TiO$_x$ layer as the initial layer.

3.3. LPCVD-TiO$_2$ on PCVD-TiO$_x$ Initial Layer

Figure 6 shows dependence of deposition rate (solid-circle) and surface roughness (open-circle) of LPCVD-TiO$_2$ layer on PCVD-TiO$_x$ initial layer thickness, where the TiO$_x$ layer and the TiO$_2$ layer was performed below 90˚C for various periods and at 360˚C for 20 min respectively. Since the TiO$_2$ layer was deposited by *in-situ* process in reactor, thickness of the TiO$_x$ layer and the TiO$_2$ layer was determined by the result of **Figure 5** and
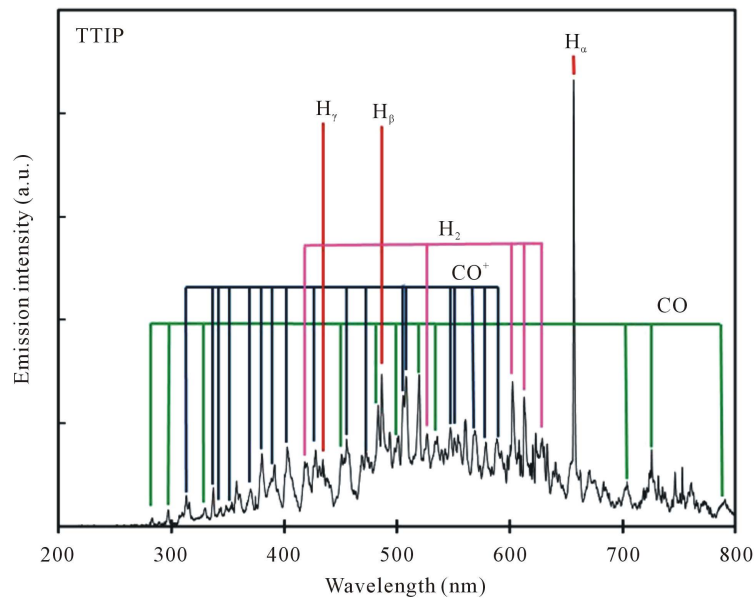
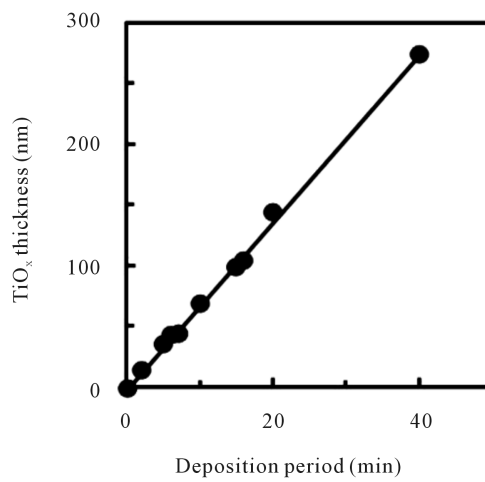**Figure 4.** Optical emission spectrum from TTIP-plasma.

Figure 5. Dependence of TiO_x thickness on deposition period by PCVD.
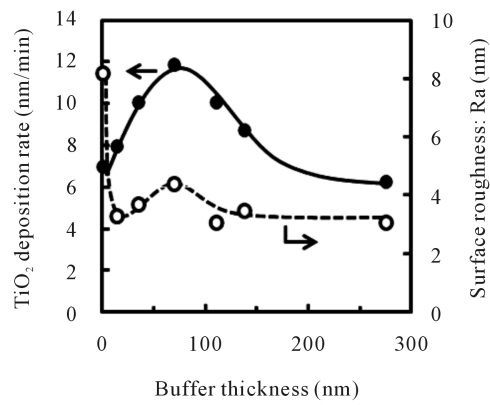

Figure 6. Dependence of LPCVD-TiO_2 deposition rate (solid-circle) and surface roughness: Ra (open-circle) on initial PCVD-TiO_x layer thickness.

by removal the TiO$_x$ thickness from the total thickness, respectively. Deposition rate of the TiO$_2$ layer about 6 nm/min on glass was significantly increased on the initial layer with the thickness and as high as 12 nm/min on 70 nm-thick initial layer, but decreased with the thickness beyond 100 nm and become similar deposition rate on glass. **Figure 7** shows θ - 2θ XRD spectra of LPCVD-TiO$_2$ layer ((a) on 275 nm-thick initial layer, (b) on 70 nm-thick initial layer, (c) on glass without the initial layer) and (e) 140 nm-thick initial layer after annealing at 360˚C for 5 min in vacuum as just before the LPCVD process. (101), (200) and (211) anatase-TiO$_2$ diffraction peaks without the peak due to another crystal phase were observed in the spectrum of the LPCVD-layer directly deposited on glass with broad spectrum around 21˚, which indicated the layer was poly-crystallized in anatase-phase. It is noted that the diffraction spectrum was similar to that of the layers deposited by using TTIP + O$_2$ and TTIP + H$_2$ [13], which indicated the guest gas such as H$_2$ and O$_2$ is not useful to control orientation of the grains. In contrast, (112) anatase-TiO$_2$ diffraction peak was also appeared for LPCVD-layer on the initial layer with the thickness of 70 nm, whereas the spectrum of LPCVD-layer on the initial layer as thick as 275 nm was similar to that for the layer directly deposited on glass. It is noted that such diffraction peaks due to anatase-TiO$_2$ was originated from the LPCVD-layer because any peaks of TiO$_2$ was not observed for the initial layer without LPCVD-layer (**Figure 7(e)**). **Figure 8** shows orientation ratio of (101), (100), (112) and (211) for the initial layer thickness, where the orientation ratio was estimated by the integrated peak intensities using the relative
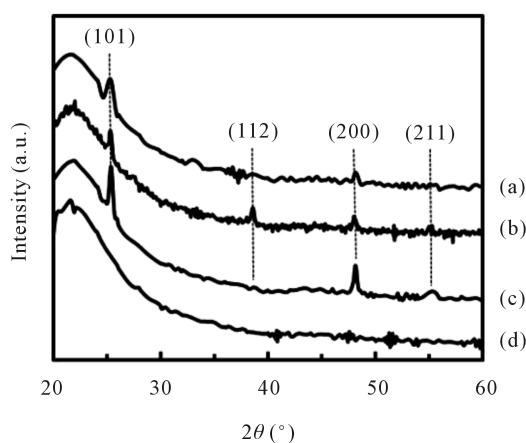

Figure 7. XRD spectra of LPCVD-TiO$_2$ deposited on (a) 275 nm-thick initial layer, (b) 70 nm-thick initial layer and (c) glass, and (d) 145 nm-thick initial layer without LPCVD-layer.
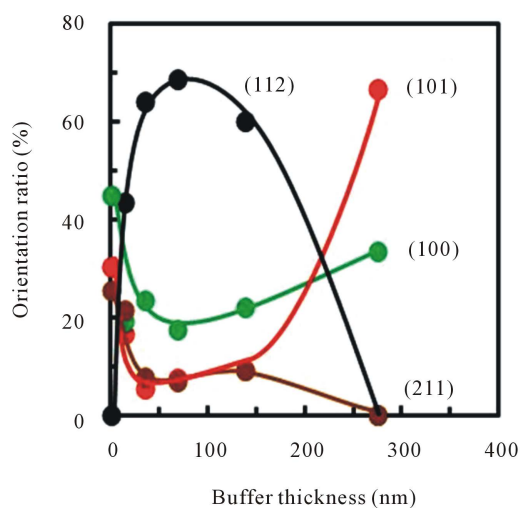

Figure 8. Dependence of orientation ratio for LPCVD-TiO$_2$ layer on initial layer thickness.

intensity of the standard powder diffraction database [16]. The orientation ratio of (112) was increased with the initial layer thickness and as high as 68% for the LPCVD-layer on 70 nm-thick initial layer, but decreased with the thickness beyond 70 nm and almost 0% on 275 nm-thick initial layer. Previously, Kim *et al.* reported deposition rate of anatase-TiO₂ layer on soda-line glass is notably increased around 360˚C with <112>-orientation ratio by CVD using TTIP [11]. Although such dependence on deposition temperature the deposition rate was not observed on Pyrex-glass in this work including previous reports of TiO₂ deposition on quartz-glass by LPCVD using TTIP + O₂ and TTIP + H₂ [12] [13], significant increased deposition rate for the highly <112>-oriented layer on the initial layer with the thickness around 70 nm were consistent with the result on Soda-lime glass. Commonly, it is considered that nuclei at the initial stage play an important role for deposition feature. In the case on low activity surface, the nucleation is dominated by clustering of partially dissociated precursor in the scheme as shown in the Section 3.1, in which the nucleation is probably performed with the low surface energy. In contrast, if the partially dissociated precursor consisting of $(RO)_xTi (OH)_{4-x}$ reacts to reactive species on the substrate surface, orientation of the nucleation is limited by the reaction. As previously reported, it is expected OH-species chemisorbed to Ti are included in the PCVD-TiO$_x$ layer deposited at such low temperatures [15]. Although the OH-species may be desorbed from the layer before the LPCVD at 360˚C, the partially dissociated precursor supplied to the surface with the residual chemisorbed-OH occurs oxolation to form $(RO)_xTi-O-TiO_x$ at the surface, which certainly control the nuclei. In the process, it is promised that the partially crystallized surface of the initial layer, which was observed as ring-pattern in halo by RHEED and the pattern was dependent on the initial layer thickness, is also important for the orientation control of LPCVD-TiO₂ because the crystallized part acts as the nuclear for TiO₂ deposition. Of course, such feature is notably dependent on atomic-arrangement at the nuclear surface, which is originated from the crystal structure and the orientation. Detailed crystallographic study at the interface between <112>-oriented TiO₂ and TiO$_x$ initial layer interface is in progress by TEM. It is mentioned here that the enhanced adsorption and reaction of the precursor at the initial stage is resulted in increase of the nuclei density. Indeed, the surface roughness of the LPCVD-layer deposited on the TiO$_x$ layer was notably decreased as shown in **Figure 6** (open-circle).

3.4. Photo-Induced Properties

Photo-induced properties on anatase-TiO₂ are generally characterized by the hydrophilicity and decomposition of organic compounds. In this study, contact angle of water after UV-irradiation and optical absorption at 633 nm in MB-solution during UV-irradiation was used to evaluate the hydrophilicity and the photocatalytic property, respectively.

Contact angle of water on LPCVD-TiO₂ layer deposited on glass (solid-circle), 70 nm-thick initial layer (open-circle) and 275 nm-thick initial layer (solid-triangle) for UV-light irradiation time were shown in **Figure 9**, in which 10 μL deionized water was dropped on the samples and 365 nm black-light with the power density of
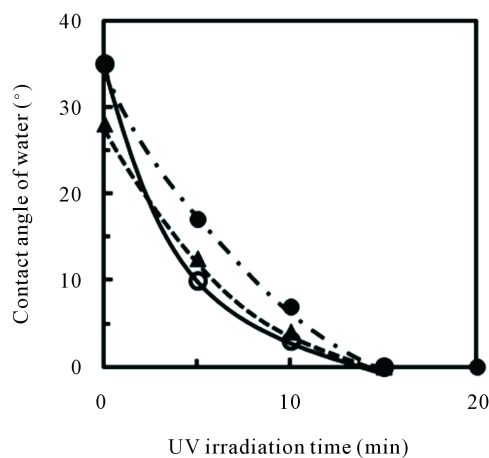

Figure 9. Variation of contact angle of water on TiO₂ layer deposited on glass (solid-circle), 70 nm-thick TiO$_x$ layer (solid-circle) and 275 nm-thick TiO$_x$ layer (solid-triangle) for UV-irradiation time.

0.5 mW/cm^2 was used as the UV-light. All samples showed super-hydrophilicity after UV-irradiation for 15 min. In general, the hydrophilicity on the TiO$_2$ is generated by photo-excited holes at the surface, which form Ti^{3+} then Ti-OH [17]. It is noted that the response for the UV-irradiation on the TiO$_2$ layer deposited on 70 nm-thick initial layer was higher than that on TiO$_2$ layer directly deposited on glass whereas the surface roughness was notably low in comparison to the layer without initial layer. Since contact angle of water is decreased with increasing surface roughness on hydrophilic material as described by Wenzel's relationship [18], the results suggests Ti-OH was more efficiently formed at the surface of the layer on 70 nm-thick initial layer than that of the layer directly deposited on glass because the roughness of the former was significantly lower than that of the latter.

Transmission of 633 nm He-Ne laser light through 200 µm-thick MB solution with the initial concentration of 2 mM during UV-irradiation are shown in **Figure 10**, in which red-, blue-, black-, green-line shows the result on TiO$_2$ layer deposited on glass, 35 nm-thick initial layer, 70 nm-thick initial layer and 275 nm-thick initial layer respectively and brown-line shows on Pyrex-glass. The initial transmittance of the MB-solution at 633 nm was about 35%, in which the molar absorption coefficient at 633 nm was obtained as 2.6×10^4 M^{-1}·cm^{-1}, and the transmission was negligibly increased within 0.3% on the glass after the UV-irradiation for 30 min. In contrast, the transmittance was increased on TiO$_2$ layer with the UV-irradiation time depending on the initial layer thickness. Previously, Zhang *et al.* indicated the decreased of absorption around 630 nm is due to degradation of MB resulting from dissociation of methyl-group by OH radicals generated by photo-excited holes on TiO$_2$ surface, in which the dissociation is owing to first-order kinetics [19]. The residual MB concentration can be estimated by the optical transmission using Lambert-Beer's Law;

$$C = \left\{ \ln \left(I_{\mathrm{o}} / I \right) \right\} \big/ \left(\varepsilon d \right),$$

where I_{o}, I, ε, d and C is the laser light intensity induced MB-solution, the transmitted light intensity, molar absorption coefficient of MB (2.6×10^4 M^{-1}·cm^{-1}), optical pass length (200 µm) and molar concentration of MB, respectively. For the increase of transmission intensity due to the decomposition via first order reaction, the MB-concentration decreasing with UV-irradiation time can be described by using rate constant (k);

$$C = C_{\mathrm{o}} \mathrm{e}^{-kt},$$

where C_{o} and t is initial MB-concentration (2 mM) and UV-irradiation time respectively. **Figure 11** shows $\ln(C/C_{\mathrm{o}})$ for UV-irradiation time, in which red-, green- and black-line is the result for the TiO$_2$ layer directly deposited on glass, on 35 nm-thick initial layer and on 70 nm-thick initial layer respectively. The increase of transmission due to clearly indicated MB-decomposition via first order kinetics. Rate constant of the decomposition was obtained as **Figure 12** for (a) the initial layer thickness and (b) <112>-orientation ratio of the
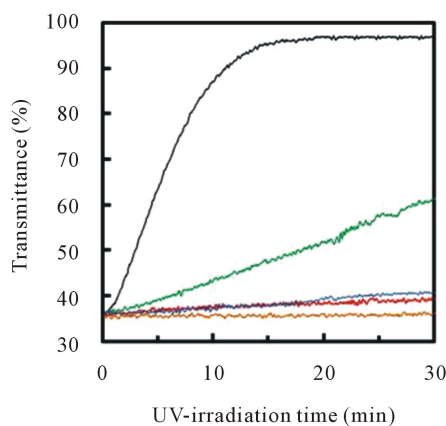

Figure 10. UV-irradiation time dependent transmittance of 633 nm He-Ne laser through 2 mM MB-solution on TiO$_2$ layer (red-line: directly deposited on glass, green-line: on 35 nm-thick TiO$_x$, black-line: on 70 nm-thick TiO$_x$, blue-line: on 275 nm-thick TiO$_x$) and without TiO$_2$ layer (brown-line).
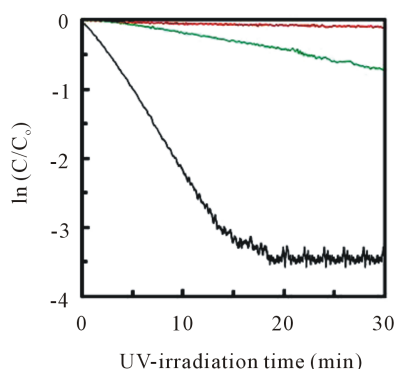
Figure 11. $\ln(C/C_o)$ plot for UV-irradiation time, where C_o and C is MB-concentration at initial and determined by the results in **Figure 10** on TiO_2 layer (red-line: directly deposited on glass, green-line: on 35 nm-thick TiO_x, brown-line: on 70 nm-thick TiO_x).
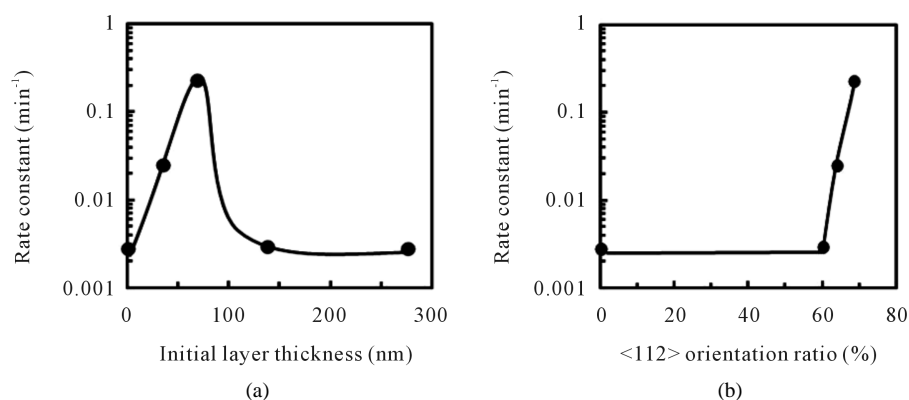

Figure 12. Dependence of rate constant for MB-decomposition obtained from the results of **Figure 11** on (a) the initial layer thickness and (b) <112>-orientation ratio of the TiO_2 layer.

LPCVD-TiO_2 layer. As reported previously, the rate constant under UV-irradiation is dependent on pH, MB-concentration, dissolved oxygen density in the solution and the irradiated UV-light power, in which the rate constant is expected to be increased around pH 4 in O_2 dissolved solution with the light power [4]. As the results, MB is decomposed with the low rate constant in the solution dissolved in pure-water without any electrolyte and O_2-bubbling. Indeed, the decomposition rate constant of 2.8×10^{-3} min^{-1} obtained by using the TiO_2 layer directly deposited on glass was lower than that of reported value (3.2×10^{-2} min^{-1}) in pH 3.8 solution by using Degussa P-25. However, the rate constant was notably increased with the initial layer thickness but steeply decreased beyond 70 nm. The maximal rate constant of 2.3×10^{-1} min^{-1} was large by two-order comparing to the value using the TiO_2 layer directly deposited on glass. It is noted that impurity from Pyrex-glass substrate was negligible because the similar rate constant ($\sim 3.2 \times 10^{-2}$ cm^{-1}) was obtained for the layer directly deposited on quartz glass. As shown in the Section 3.3, orientation ratio of grains in the TiO_2 layer was dependent on the initial layer thickness. **Figure 12(b)** shows the rate constant for the <112>-orientation ratio. The rate constant was not dependent on the <112>-orientation ratio below 60% but drastically increased with the ratio beyond 60%. The result indicates MB-decomposition is seemed to be enhanced by the <112>-oriented grains as previously reported [10] [11] but not simply dependent on the orientation ratio. It has been generally believed that organic compound is decomposed by the oxidation contributed surface trapped hydroxyl radical which is formed by photo-excited holes, where photo-excited electrons act to form reduced O_2 which are consumed to product hydrogen-peroxides and hydroxyl-ions [19]. Of course, the both reactions for redox in solution are necessary for successive photocatalytic-organic-decomposition. However, it is considered that one type of photo-excited carriers either the electron or hole is drifted to the surface on bulk semiconductor due to band-bending at the surface. Poly-crystalline semiconductor is including some different oriented surfaces, in which the defect level and density is probably different on each surfaces. Therefore, the band-bending is dependent on the orientation with

the effective carrier density in the grain. If the oxidation or the reduction in solution is selectively or mainly occurred on each oriented surfaces and the carriers is transported between the grains, effective reaction at the surfaces can be achieved by using poly-crystalline semiconductor. Indeed, the LPCVD-TiO₂ layer showed n-type conductivity with the resistivity 1 - 4 Ωcm, in which the degenerated grains due to so high carrier density were interconnected by tunneling conduction across the grain-boundaries as well as LPCVD-TiO₂ layer deposited in TTIP + H₂ ambient [13]. As the result, it is predicted that the band-bending of <112>-oriented anatase-TiO₂ surface is quite different from the other oriented surfaces.

4. Conclusion

TiO$_x$ layer deposited on glass-substrate as amorphous phase by PCVD at low temperature below 90°C was used as initial layer to control orientation of anatase-TiO₂ layer by LPCVD at 360°C using TTIP-single precursor. Poly-crystalline anatase-TiO₂ layer with <112>-orientation ratio as high as 68% was obtained on the initial layer with optimized thickness about 70 nm. Super-hydrophilicity was confirmed on the all LPCVD-TiO₂ layers including without the initial layer but the response to UV-irradiation was high on the highly <112>-oriented TiO₂ layer. UV photo-induced organic decomposition was demonstrated in 200 μm-thick MB-solution with monitoring transmission of He-Ne laser light. The result showed that the decomposition was according to first order kinetics and the rate constant was notably dependent on the initial layer thickness, in which the rate constant was as high as 2.3×10^{-1} min^{-1} on the TiO₂ layer on the 70 nm-thick initial layer whereas the constant was 2.8×10^{-3} min^{-1} on the TiO₂ layer directly deposited on glass. The result of rate constant depending on <112>-orientation ratio, in which the decomposition was enhanced by <112>-oriented surface but not simply dependent on increase of the orientation ratio, speculated carrier transport across the grain-boundaries was also concerned with the efficient decomposition. In the future study, the predicted surface reaction scheme including the photo-excited carrier transport phenomena will be disclosed by electro-chemical measurements such as ζ-potential in solution and details of the crystallographic analysis such as TEM.

References

[1]   Wang, R., Hashimoto, K. and Fujishima, A. (1997) Light-Induced Amphiphilic Surfaces. *Nature*, **388**, 431-432. http://dx.doi.org/10.1038/41233

[2]   Mills, A., Lepre, A., Elliott, N., Bhopal, A., Parkin, I.P. and Neill, S.A. (2003) Characterisation of the Photocatalyst Pilkington Activ™: A Reference Film Photocatalyst? *Journal of Photochemistry and Photobiology A*: *Chemistry*, **160**, 213-224. http://dx.doi.org/10.1016/S1010-6030(03)00205-3

[3]   Koelsch, M., Cassaignon, S., Guillemoles, J.F. and Joivet, J.P. (2002) Comparison of Optical and Electrochemical Properties of Anatase and Brookite TiO₂ Synthesized by the Sol-Gel Method. *Thin Solid Films*, **403-404**, 312-319. http://dx.doi.org/10.1016/S0040-6090(01)01509-7

[4]   Zhang, T., Oyama, T., Aoshima, A., Hidaka, H., Zhao, J. and Serpone, N. (2001) Photooxidative N-Demethylation of Methylene Blue in Aqueous TiO₂ Dispersions under UV Irradiation. *Journal of Photochemistry and Photobiology A*: *Chemistry*, **140**, 163-172. http://dx.doi.org/10.1016/S1010-6030(01)00398-7

[5]   Chang, H., Su, C., Lo, C.H., Chen, L.C., Tsung, T.T. and Jwo, C.S. (2004) Photodecomposition and Surface Adsorption of Methylene Blue on TiO₂ Nanofluid Prepared by ASNSS. *Materials Transactions*, **45**, 3334-3337. http://dx.doi.org/10.2320/matertrans.45.3334

[6]   Gotić, M., Ivanda, M., Sekulić, A., Musić, S., Popovi, S., Turković, A. and Furić, K. (1996) Microstructure of Nano-sized TiO₂ Obtained by Sol-Gel Synthesis. *Material Letters*, **28**, 225-229. http://dx.doi.org/10.1016/0167-577X(96)00061-4

[7]   Lobl, P., Huppertz, M. and Mergel, D. (1994) Nucleation and Growth in TiO₂ Films Prepared by Sputtering and Evaporation. *Thin Solid Films*, **251**, 72-79. http://dx.doi.org/10.1016/0040-6090(94)90843-5

[8]   Gauthier, V., Bourgeois, S., Sibillot, P., Maglione, M. and Sacilotti, M. (1999) Growth and Characterization of AP-MOCVD Iron Doped Titanium Dioxide Thin Films. *Thin Solid Films*, **340**, 175-182. http://dx.doi.org/10.1016/S0040-6090(98)01469-2

[9]   Nakamura, M., Kobayashi, M., Kuzuya, N., Komatsu, T. and Mochizuka, T. (2005) Hydrophilic Property of SiO₂/TiO₂ Double Layer Films. *Thin Solid Films*, **502**, 121-124. http://dx.doi.org/10.1016/j.tsf.2005.07.254

[10] Tokita, S., Takana, N. and Saitoh, H. (2000) High-Rate Epitaxy of Anatase Films by Atmospheric Chemical Vapor Deposition. *Japanese Journal of Applied Physics*, **39**, L169-L171. http://dx.doi.org/10.1143/jjap.39.l169

[11] Kim, B., Byun, D., Kee, J. and Park, D. (2002) Structural Analysis on Photocatalytic Efficiency of TiO₂ by Chemical

Vapor Deposition. *Japanese Journal of Applied Physics*, **41**, 222-226. http://dx.doi.org/10.1143/JJAP.41.222

[12] Yamauchi, S., Saiki, S., Ishibashi, K., Nakagawa, A. and Hatakeyama, S. (2014) Low Pressure Chemical Vapor Deposition of Nb and F Co-Doped TiO$_2$ Layer. *Journal of Crystallization Process and Technology*, **4**, 79-88. http://dx.doi.org/10.4236/jcpt.2014.42011

[13] Yamauchi, S., Ishibashi, K. and Hatakeyama, S. (2014) Low Pressure Chemical Vapor Deposition of TiO$_2$ Layer in Hydrogen-Ambient. *Journal of Crystallization Process and Technology*, **4**, 185-192. http://dx.doi.org/10.4236/jcpt.2014.44023

[14] Shmakov, A.G., Korobeinichev, O.P., Knyazkov, D.A., Paletsky, A.A., Maksutov, R.A., Gerasimov, I.E., Bolshova, T.A., Kiselev, V.G. and Gritsan, N.P. (2013) Combustion Chemistry of Ti(OC$_3$H$_7$)$_4$ in Premixed Flat Burner-Stabilized H$_2$/O$_2$/Ar Flame at 1 atm. *Proceedings of the Combustion Institute*, **34**, 1143-1149. http://dx.doi.org/10.1016/j.proci.2012.05.081

[15] Yamauchi, S., Suzuki, H. and Akutsu, R. (2014) Plasma-Assisted Chemical Vapor Deposition of Titanium Oxide Layer at Room-Temperature. *Journal of Crystallization Process and Technology*, **4**, 20-26. http://dx.doi.org/10.4236/jcpt.2014.41003

[16] Weisssmann, S., *et al.* (1978) Selected Powder Diffraction Data for Metals and Alloys, JCPDS, Card No. 21-1272.

[17] Sakai, N., Fujishima, A., Watanabe, T. and Hashimoto, K. (2003) Quantitative Evaluation of the Photoinduced Hydrophilic Conversion Properties of TiO$_2$ Thin Film Surfaces by the Reciprocal of Contact Angle. *The Journal of Physical Chemistry B*, **107**, 1028-1035. http://dx.doi.org/10.1021/jp022105p

[18] Wenzel, R.W. (1936) Resistance of Solid Surfaces to Wetting by Water. *Industrial and Engineering Chemistry*, **28**, 988-994. http://dx.doi.org/10.1021/ie50320a024

[19] Hoffmann, M.R., Martin, S.T., Choi, W. and Bahnemann, D.W. (1995) Environmental Applications of Semiconductor Photocatalysis. *Chemical Reviews*, **95**, 69-96. http://dx.doi.org/10.1021/cr00033a004